

Alloxan under pressure—squeezing an extremely dense molecular crystal structure

SUPPLEMENTARY INFORMATION

Nicholas P. Funnell,^{*a} Craig L. Bull,^a Christopher J. Ridley,^a
Simon Parsons^b and James P. Tellam^a

^a ISIS Facility, Rutherford Appleton Laboratory, Harwell Science and Innovation Campus,
Didcot, OX11 0QX, UK

^b EaStCHEM School of Chemistry and Centre for Science at Extreme Conditions,
University of Edinburgh, The King's Buildings, West Mains Road, Edinburgh, EH9 3FJ, U.K.

*To whom correspondence should be addressed;

E-mail: nick.funnell@stfc.ac.uk

Contents

1	Experimental details	3
1.1	Sample preparation	3
1.2	High-pressure neutron diffraction measurements	3
1.3	Rietveld refinement	3
1.4	High-pressure Raman spectra for hydrogenated alloxan	4
2	Neutron powder patterns and refinement statistics	5
3	High-pressure Raman spectra	10
4	Computational details	11
4.1	Intermolecular energy calculations	11
4.2	Geometry optimisations	11
5	Packing coefficients	13
6	Ring stacking analysis	14
7	Nearest-neighbour compression video notes	15
8	References	16

1 Experimental details

1.1 Sample preparation

Alloxan monohydrate, deuterium oxide and methanol-OD were purchased from Sigma Aldrich, and used without purification. **Alloxan-h₂**: alloxan monohydrate (5.00 g) was sublimed (240°C, 2 Torr) to produce yellow crystals. This was repeated twice more to yield pure alloxan (4.00 g). **Alloxan-d₂**: alloxan monohydrate (3.50 g) was dried under vacuum at 80°C overnight. The dried alloxan was stirred in D₂O (50 mL) at 40°C for 1 week. D₂O was removed by freeze drying, and this procedure was subsequently repeated. The resulting residue was dissolved in MeOD (50 mL) and heated to 40°C for 24 hours before concentrating *in vacuo*. Purification was achieved by sublimation (240°C, 2 Torr) to produce yellow crystals. This was repeated twice more to yield alloxan-d₂ (2.50 g); ¹H NMR analysis showed a 76% deuterium incorporation.

The deuterated alloxan sample was loaded into a null-scattering TiZr gasket, along with a lead pellet to act as a pressure marker. The gasket was placed between tungsten carbide anvils inside a clamp device, designed for use with gas loading apparatus.^{S1} The clamp was left unsealed, and placed in the gas loader. The gas loader chamber was then filled with argon gas, compressed to ca. 2 kbar. The clamp was sealed shut, removed from the gas loader, and placed in an oil-driven Paris–Edinburgh press.

1.2 High-pressure neutron diffraction measurements

High-pressure, room-temperature, diffraction data were collected on the PEARL instrument^{S2} at the ISIS Neutron and Muon Facility, using the time-of-flight method. The first dataset measured the as-loaded clamp. Following this, data were collected at 15 tonnes of applied oil load, and then at successive 5 tonne increments up to 35 tonnes, and then at 10 tonne increments up to 75 tonnes. The pressure inside the clamp was measured via a Birch-Murnaghan equation of state, previously determined for lead.^{S3} Diffraction data were corrected for attenuation by the anvils, detector efficiency, and incident beam flux, using Mantid.^{S4}

1.3 Rietveld refinement

Rietveld refinements were carried out using Topas Academic 6.0.^{S5} Molecular geometry was described using a Z-matrix, where bond distances/angles were taken from a previous high-quality neutron diffraction study (CSD refcode: ALOXAN14).^{S6} A rigid-body approach was used for the refinement, keeping the molecular geometry fixed, and allowing translation and rotation parameters to refine (where permitted by symmetry). Sites for hydrogen and deuterium atoms were included on each molecule, allowing a 0.1 Å difference for N–H(D) bond distance. All data were refined simultaneously, with a single, global, parameter for hydrogen/deuterium occupancy which indicated a deuteration level of approximately 25%. The discrepancy between deuteration level in the refinement and the ¹H NMR analysis, following initial synthesis, may have been due to atmospheric partial H/D exchange. This could have occurred during sample loading, as the preparation of the gas clamp equipment leads to the sample being exposed to atmospheric conditions for several minutes. At each pressure, a single isotropic displacement parameter was refined for all carbon atoms, and also for all nitrogen atoms. Displacement parameters for the oxygen and hydrogen/deuterium atoms were constrained to 1.5× the value of their parent C/N atom—this value was approximately the ratio observed in a preliminary refinement of the alloxan structure, measured in a vanadium can (not reported here). Above 30 tonnes, the displacement parameters could not be stably refined and so they were held fixed to the values determined at 30 tonnes.

1.4 High-pressure Raman spectra for hydrogenated alloxan

Alloxan-h₂ was loaded in a Merrill–Bassett diamond anvil cell (DAC) equipped with 600 μm-culet diamonds, tungsten-carbide Boehler-Almax backing seats, and a tungsten gasket. The sample chamber was machined via spark erosion. Along with the sample, a ruby chip was included for pressure measurement, and a 1:1 (by volume) pentane-isopentane mixture. The cell pressure was determined by the ruby fluorescence method. Raman data were collected on bespoke apparatus, using a Princeton Instruments SP2500i spectrometer with 1800 g holographic and 1200 g blaze gratings. The sample was irradiated using a diode laser ($\lambda = 532$ nm). All data were collected at room temperature.

2 Neutron powder patterns and refinement statistics

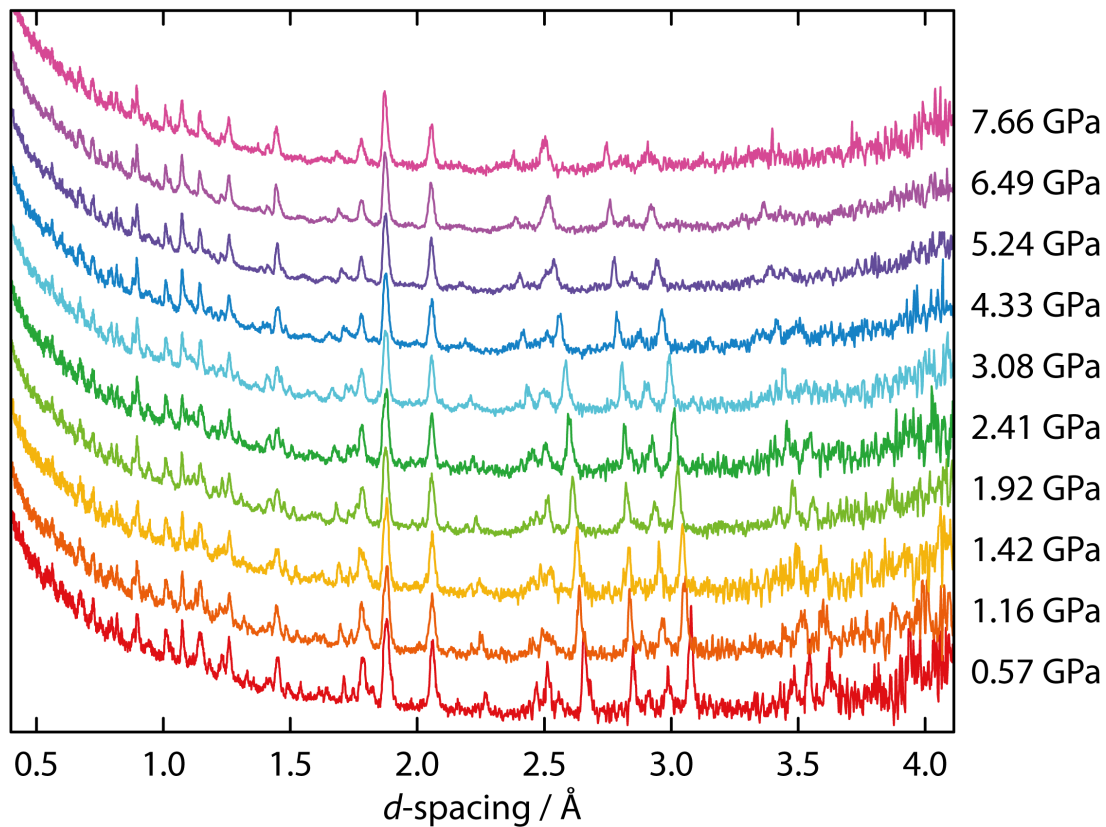


Figure S1: As-measured neutron powder patterns, showing the full data range collected at all pressure points. All fits to these data, over a truncated range, are given further below. In addition to sample reflections, contaminant reflections can be attributed to the lead pressure marker, tungsten carbide anvils, and nickel, which is present as a binder material in the anvils.

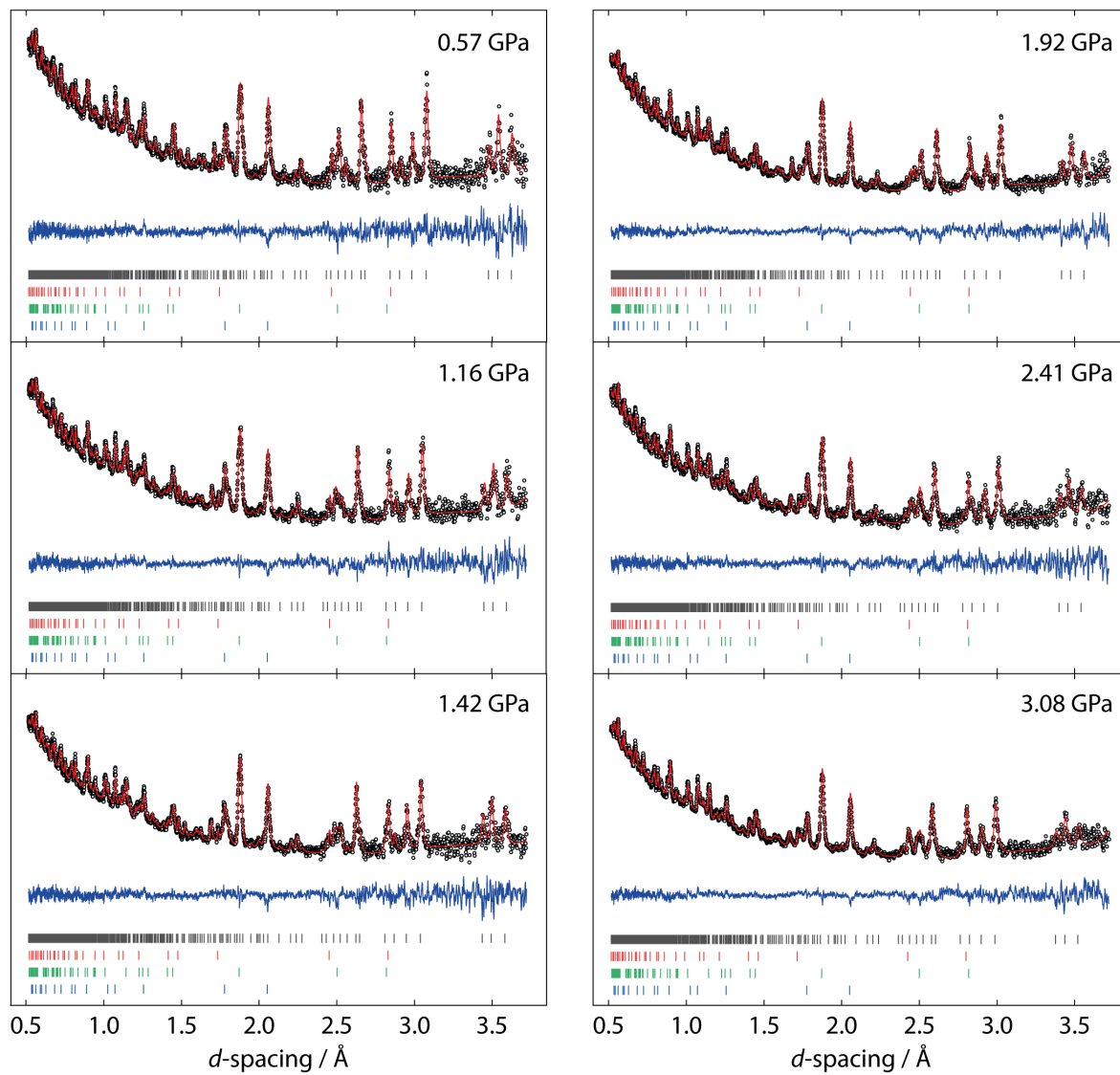


Figure S2: Rietveld fits against high-pressure neutron powder data. The y-axis shows intensity in arbitrary units—all data are shown on the same scale. Data are shown as open circles, the fitted Rietveld profile in red and the residual in blue. Tickmarks from top to bottom: black—alloxan; red—lead pressure marker; green—tungsten carbide; blue—nickel.

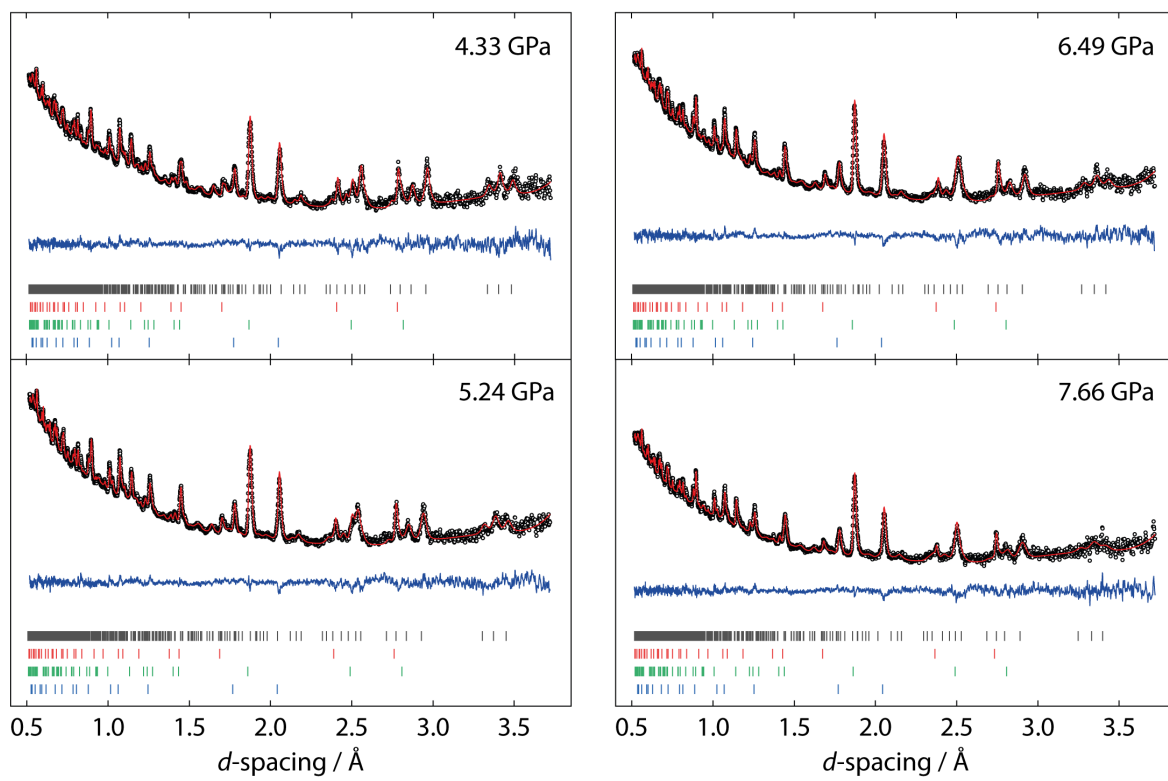


Figure S2: continued.

Table S1: Crystallographic refinement details for all pressure points. The uppermost pressure of 7.66 GPa is included here for information. All data are collected at room temperature.

Pressure / GPa	0.57(2)	1.163(18)	1.42(2)	1.922(15)	2.41(2)
Formula	$C_4O_4N_2H_{0.75}D_{0.25}$	$C_4O_4N_2H_{0.75}D_{0.25}$	$C_4O_4N_2H_{0.75}D_{0.25}$	$C_4O_4N_2H_{0.75}D_{0.25}$	$C_4O_4N_2H_{0.75}D_{0.25}$
Spacegroup	$P4_12_12$	$P4_12_12$	$P4_12_12$	$P4_12_12$	$P4_12_12$
a-axis / Å	5.8059(8)	5.7580(7)	5.7382(7)	5.7051(6)	5.6753(10)
c-axis / Å	13.905(2)	13.794(2)	13.747(2)	13.6603(17)	13.593(3)
Volume / Å ³	468.73(15)	457.33(14)	452.63(13)	444.62(10)	437.84(17)
Density / gcm ⁻³	2.020	2.071	2.092	2.130	2.163
Packing coefficient	0.835	0.849	0.852	0.863	0.876
Parameters	42	42	42	42	42
Data points	3291	3291	3291	3291	3291
R_{wp}	3.244	3.170	3.163	2.539	3.276
Goodness of fit	0.765	0.823	0.814	0.918	0.827
Pressure / GPa	3.075(16)	4.33(2)	5.24(2)	6.48(2)	7.66(3)
Formula	$C_4O_4N_2H_{0.75}D_{0.25}$	$C_4O_4N_2H_{0.75}D_{0.25}$	$C_4O_4N_2H_{0.75}D_{0.25}$	$C_4O_4N_2H_{0.75}D_{0.25}$	$C_4O_4N_2H_{0.75}D_{0.25}$
Spacegroup	$P4_12_12$	$P4_12_12$	$P4_12_12$	$P4_12_12$	$P4_12_12$
a-axis / Å	5.6443(8)	5.5997(10)	5.5604(12)	5.5308(15)	5.503(2)
c-axis / Å	13.507(2)	13.351(3)	13.245(4)	13.126(4)	13.030(6)
Volume / Å ³	430.30(14)	418.64(18)	409.5(2)	401.5(2)	394.6(4)
Density / gcm ⁻³	2.201	2.262	2.312	2.359	2.391(2)
Packing coefficient	0.888	0.902	0.913	0.922	0.931
Parameters	40	40	40	40	40
Data points	3291	3291	3291	3291	3291
R_{wp}	2.599	2.716	2.494	2.599	2.716
Goodness of fit	0.916	0.975	1.017	1.043	0.975

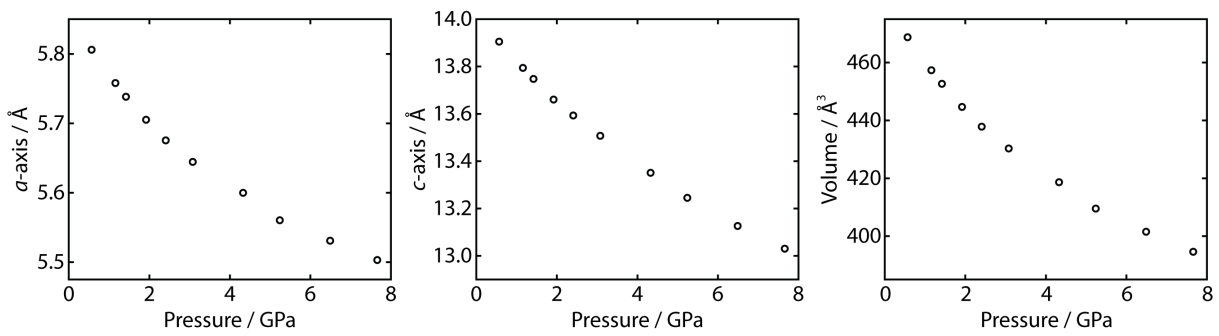


Figure S3: Cell axes and volume from Table 1, plotted as a function of pressure. All error bars are within the size of the data markers.

3 High-pressure Raman spectra

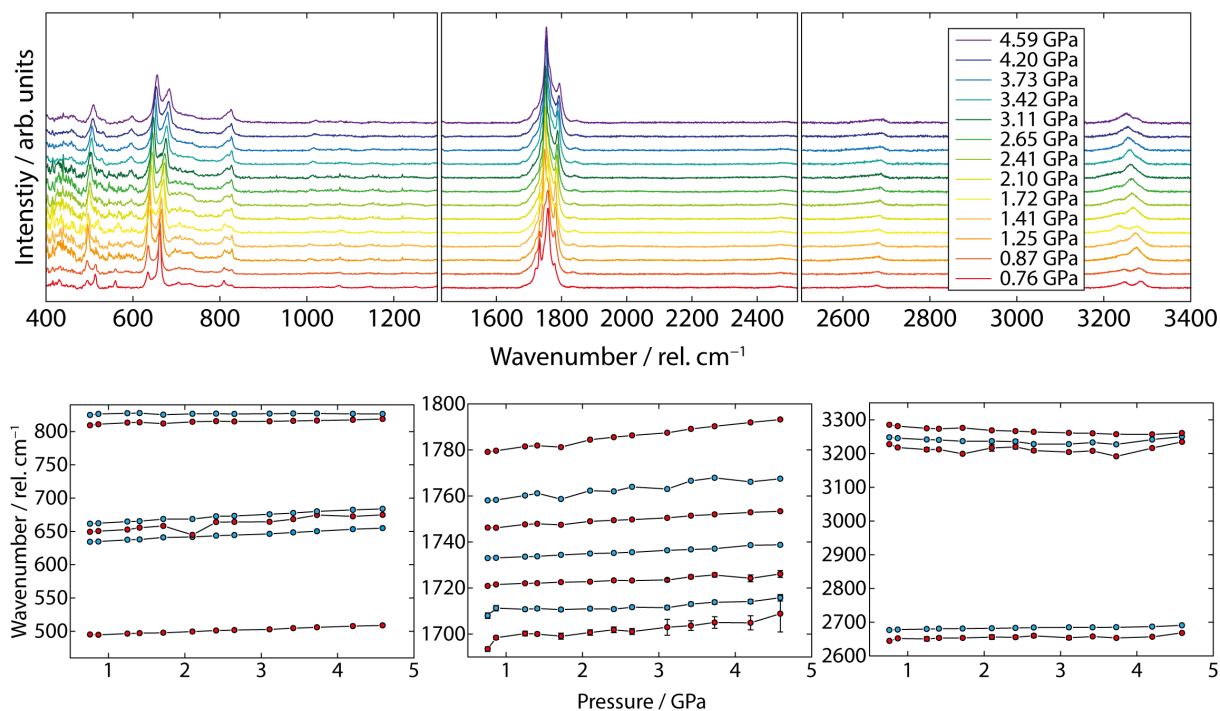


Figure S4: Top: background-corrected Raman spectra of isotopically-normal alloxan, stacked as a function of pressure between 0.76–4.59 GPa. Measurements were made over three spectral regions, each shown in individual plots from left to right. Difficulties in consistent sample focussing with changing pressure led to some spectral features being hard to follow across the full pressure range investigated here. This is particularly apparent below ca. 600 rel. cm⁻¹. Bottom: Fitted Lorentzian peak positions, as a function of pressure. The three spectral regions are shown separately (left to right); note the differing y-axis scales in each case. In the majority of cases, the positional error is within the size of the data marker. Lines connecting datapoints, and the colours used, are to aid visual clarity.

4 Computational details

4.1 Intermolecular energy calculations

PIXEL calculates molecule–molecule energies, which can be broken down into individual Coulombic, polarisation, repulsive, and dispersive components. Details of the underlying PIXEL theory/approach are given elsewhere.^{S7, S8} Difficulties arise where point and space group symmetry elements coincide, resulting in $Z' < 1$. For all our refined structures, the symmetry was first lowered to $P4_1$, so that $Z' = 1$. Furthermore, PIXEL treats atom sites as being fully occupied, so we opted to remove the deuterium atoms, leaving only the hydrogen, as it was the majority site. Electron density of the alloxan molecule was calculated using Gaussian16^{S9} at the MP2 level of theory, using a 6-31G** basis set. PIXEL calculations were performed over a 15 Å radius, using a pixel condensation level of 4. The PIXEL energies are plotted in Figure S5.

CrystalExplorer calculations^{S10} used the same input CIFs as for PIXEL, where symmetry was lowered to $P4_1$, and deuterium atoms removed. Any molecule within 6 Å of any atom on the central alloxan molecule was included in the calculation. Increasing this radius further made no difference to the final calculated energies. Intermolecular energies were calculated using the Tonto package at the B3LYP level, using a 6-31G** basis set. CrystalExplorer scales each of the Coulombic, polarisation, dispersion and repulsion terms by an empirical coefficient to account for differences between the calculated energies and those from higher-level quantum mechanical calculations, determined for a training set of crystal structures. We have plotted both the as-calculated, and scaled, energy values in Figure S5.

Symmetry-adapted perturbation theory (SAPT) calculations^{S11, S12} were carried out using the PSI4 code^{S13} using the 2+3 method,^{S14, S15} with a aug-cc-pvdz basis set. Only the highest and lowest pressure points were calculated for comparison against the PIXEL and CrystalExplorer energies. In the majority of cases, the SAPT calculations showed more stabilising Coulombic, polarisation, and dispersive energies, and more destabilising repulsive energies, than the PIXEL/CrystalExplorer-calculated energies, which show much better agreement with each other. The SAPT energies are also plotted in Figure S5.

4.2 Geometry optimisations

Geometry optimisations were carried out density functional theory, as implemented in CASTEP 18.1.^{S16} Two approaches were used—one with the unit cell held fixed, the other where the cell was allowed to optimise. In both scenarios, atomic coordinates were allowed to optimise, and $P4_12_12$ space group symmetry was applied. The refined crystal structures were used to inform the starting cell parameters and cell coordinates. The PBE exchange–correlation functional,^{S17} Grimme correction scheme for dispersion,^{S18} and on-the-fly pseudopotentials were used. A plane wave cutoff energy of 1150 eV and k -point spacing of 0.07 \AA^{-1} were used. Tolerance criteria were set as follows: maximum energy per atom $5 \times 10^{-6} \text{ eV \AA}^{-3}$, maximum force $1 \times 10^{-3} \text{ eV \AA}^{-3}$, maximum displacement $5 \times 10^{-4} \text{ \AA}$, and maximum stress $2 \times 10^{-2} \text{ GPa}$.

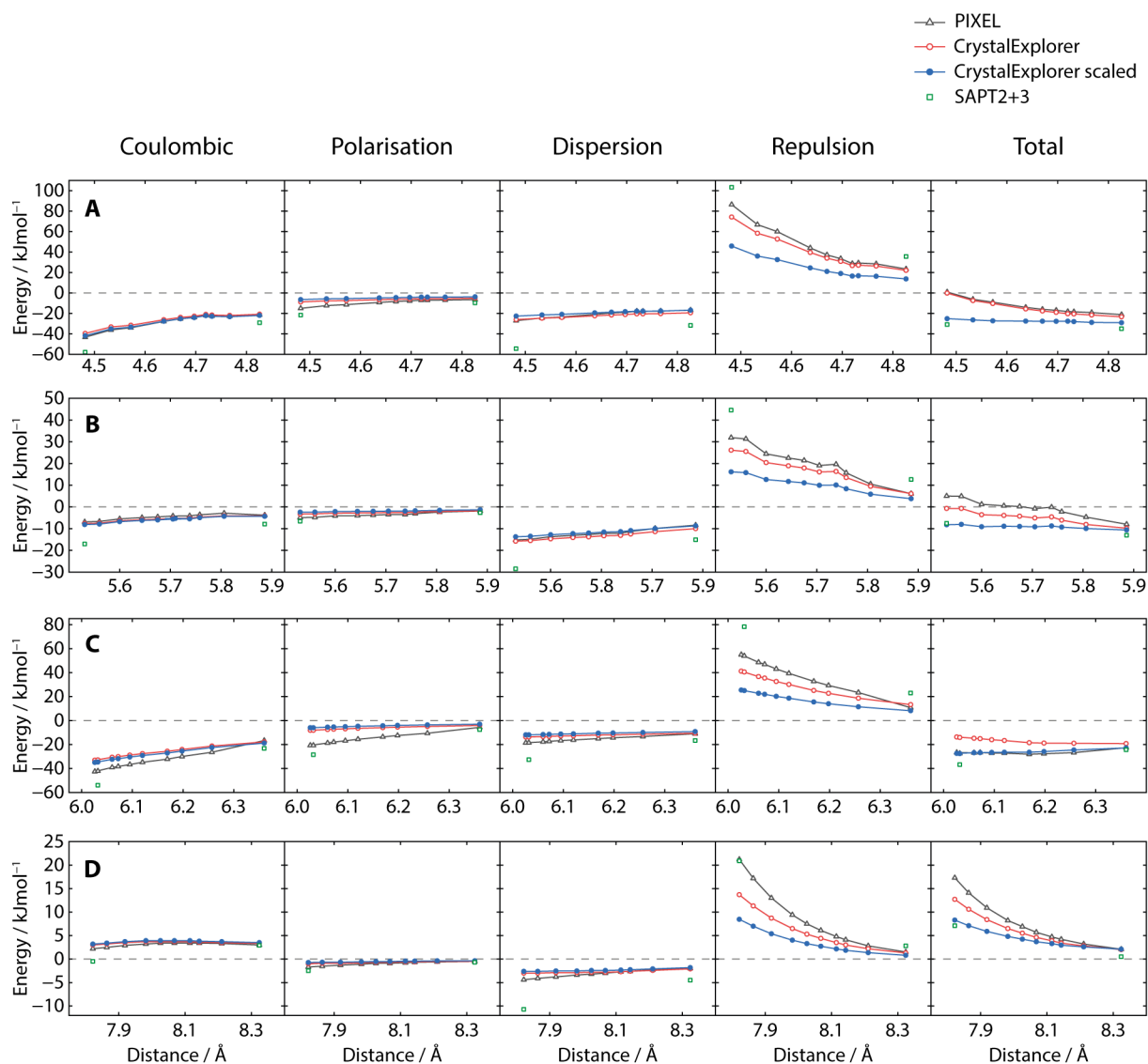


Figure S5: Comparison of intermolecular energies, calculated using PIXEL (triangles), CrystalExplorer (circles), and SAPT (squares) approaches. Only the highest and lowest pressure points are given for the SAPT calculations. Both as-calculated, and scaled, CrystalExplorer energies are given, shown as open red and filled blue circles, respectively. Each row corresponds to one of the interactions **A–D** (see main manuscript) and each column corresponds to an energy component, contributing to each interaction. All lines connecting points are not physically meaningful, but are given as a guide to the eye. The grey dotted line in each plot indicates zero energy—the dividing line between stabilising and destabilising energies. Different x- and y-axes are used for each interaction.

5 Packing coefficients

Kitaigorodskii packing coefficients C_K for C_{2v} molecules crystallising in $P4_12_12$ or $P4_32_12$ space groups. The list of crystal structures presented here is compiled from a combination other papers.^{S19–21} All C_K values are calculated using PLATON.^{S22}

Compound	CSD Refcode	C_K
Alloxan	ALOXAN	0.809
Pyridine	PYRDNA08	0.760*
Cyclopentene-1,2,3-trione	CIMNUH	0.742
Pyridine-N-oxide	PYRDNO11	0.735
Pentachloropyridine	PCLPYR	0.700
Fluorobenzene	FACFAQ	0.691
Benzonitrile	BZONTR	0.679
Pyridinium fluoride	DEHSIS10	0.675
Furan	FURANE10	0.667
Borazine	LIKSIH01	0.639

*Structure determined at 1.55 GPa

6 Ring stacking analysis

Centroid–centroid distances, and angle between mean planes, for nearest-neighbour alloxan molecules, as a function of pressure. All values are calculated using PLATON^{S22} where carbon and nitrogen atoms are used for the calculation of each centroid/plane. The centroid–centroid compression behaviour is linear. The angle between the mean planes of neighbouring molecules is dependent on this distance and the limited orientational freedom of the molecules, only being able to rotate about the 2-fold axis aligned with the [110] direction. After an initial decrease (increase in co-planarity) in the angle between mean planes, it increases slightly and then becomes invariant with pressure. At all pressures above 1.42 GPa any apparent changes are not significant as respective Δ/σ values are < 3 .

Pressure	Centroid distance / Å	Mean plane angle / °
0.57	4.762(3)	56.5(3)
1.16	4.728(3)	54.8(2)
1.42	4.715(3)	53.8(2)
1.92	4.692(2)	54.72(18)
2.41	4.665(3)	54.6(3)
3.08	4.632(3)	54.99(19)
4.33	4.568(3)	55.4(2)
5.24	4.529(3)	54.6(2)
6.49	4.478(3)	55.2(2)

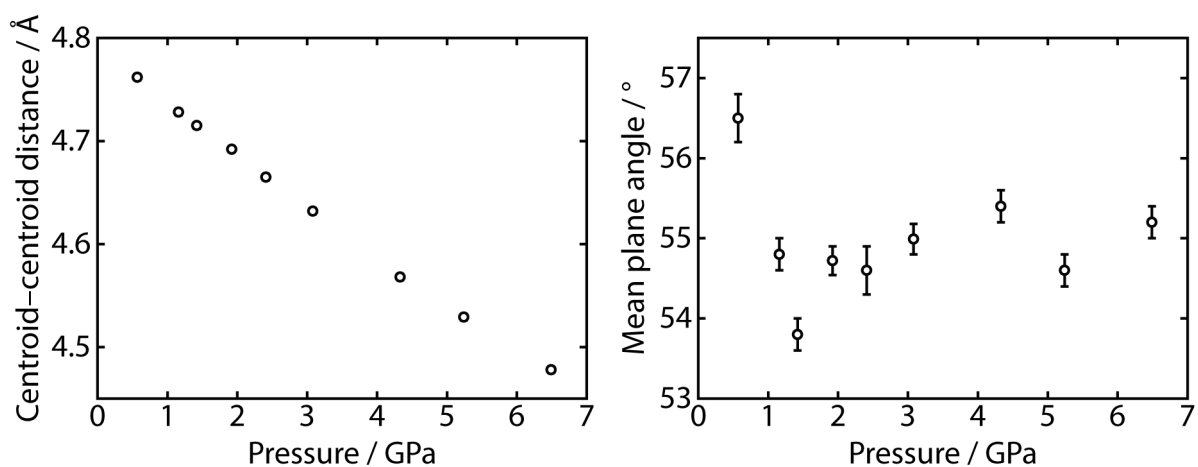


Figure S6: Centroid–centroid distance (left) and angle between ring mean planes (right) of alloxan molecules, as a function of pressure. Error bars are within the size of the data marker where not visible.

7 Nearest-neighbour compression video notes

The supplementary video 'Alloxan high-pressure.avi' animates the spatial relationship between nearest-neighbour molecules (interaction **A** in the manuscript), as a function of pressure. Carbon atoms are shown in grey, hydrogen in white, oxygen in red, and nitrogen in blue. Each pressure is shown on a separate frame, where a breakdown of the PIXEL-calculated energies are given. In addition to the absolute energies, an additional column shows energies relative to those on the first video frame (0.57 GPa); negative changes indicate increased stabilisation, and positive show decreasing stability. The geometric relationship between the molecules is given in the previous section 'Ring stacking analysis'.

8 References

- (S1) S. Klotz, J. Philippe, C. L. Bull, J. S. Loveday, R. J. Nelmes, *High Pressure Res.* **33**, 214 (2013).
- (S2) C. L. Bull, *et al.*, *High Pressure Res.* **36**, 493 (2016).
- (S3) F. Birch, *Phys. Rev.* **71**, 809 (1947).
- (S4) O. Arnold, *et al.*, *Nucl. Instrum. Meth. A* **764**, 156 (2014).
- (S5) A. Coelho, Topas V6.0 (2016).
- (S6) R. M. Ibberson, *et al.*, *CrystEngComm* **10**, 465 (2008).
- (S7) A. Gavezzotti, *Z. Kristallogr.* **220**, 499 (2005).
- (S8) A. Gavezzotti, *Molecular Aggregation: Structure Analysis and Molecular Simulation of Crystals and Liquids* (Oxford University Press, Oxford, UK, 2007).
- (S9) M. J. Frisch, *et al.*, Gaussian16, Revision B01 (2016).
- (S10) M. J. Turner, *et al.*, *CrystalExplorer17*, University of Western Australia (2017).
- (S11) A. J. Stone, *The Theory of Intermolecular Forces* (Oxford University Press, Oxford, UK, 2013).
- (S12) B. Jeziorski, R. Moszynski, K. Szalewicz, *Chem. Rev.* **94**, 1887 (1994).
- (S13) J. M. Turney, *et al.*, *Wiley Interdiscip. Rev.: Comput. Mol. Sci.* **2**, 556 (2012).
- (S14) E. G. Hohenstein, C. D. Sherrill, *J. Chem. Phys.* **133**, 104107 (2010).
- (S15) E. G. Hohenstein, C. D. Sherrill, *Wiley Interdiscip. Rev.: Comput. Mol. Sci.* **2**, 304 (2012).
- (S16) S. J. Clark, *et al.*, *Z. Krist.* **220**, 567 (2005).
- (S17) J. P. Perdew, K. Burke, E. M., *Phys. Rev. Lett.* **77**, 3865 (1996).
- (S18) S. Grimme, *J. Comput. Chem.* **27**, 1787 (2006).
- (S19) J. D. Dunitz, W. B. Schweizer, *CrystEngComm* **9**, 266 (2007).
- (S20) S. Crawford, *et al.*, *Angew. Chem. Int. Ed.* **48**, 755 (2009).
- (S21) M. A. Spackman, J. J. McKinnon, D. Jayatilaka, *CrystEngComm* **10**, 377 (2008).
- (S22) A. L. Spek, *J. Appl. Crystallogr.* **36**, 7 (2003).